C. R. Mecanique 347 (2019) 382–388

Contents lists available at ScienceDirect

Comptes Rendus Mecanique

www.sciencedirect.com

Patterns and dynamics: homage to Pierre Coullet / *Formes et dynamique : hommage à Pierre Coullet*

A brittle material with tunable elasticity: Crêpe paper

Nicolas Vandenberghe *, Emmanuel Villermaux

Aix Marseille Université, CNRS, Centrale Marseille, IRPHE, Marseille, France

ARTICLE INFO

Article history:
Received 18 January 2019
Accepted 22 February 2019
Available online 12 April 2019

Keywords:
Patterns
Fracture

ABSTRACT

We study the mechanical response, and tearing features of crêpe paper, a two-dimensional, very anisotropic material, with one direction much less stiff than the other one. Depending on how the soft direction has been pre-stretched or not, the apparent Young modulus of the material can be varied over a broad range, while its fracture energy remains unaltered. The classical *tearing concertina* problem shows that a macroscopic measurement (the shape of the teared region) provides a direct access to the fracture properties of the material (effective Young's modulus, and fracture energy). The overall discussion is conducted in the frame of Griffith's theory of fracture.

1. Introduction

When strongly stressed, a sample of a solid material breaks into pieces by the formation and extension of cracks. As multiple cracks develop and extend, the stress field is modified, and, in return, the paths followed by the cracks are altered [1–3]. In other words, cracks mutually interact and this interaction is mediated by the stress field in the sample, which may also incorporate a component of noise, either thermal, or intrinsic (see [4] and references therein). The prediction of the motion of a single crack tip in a general stress field remains a challenging problem [5,6] and no simple law offering a "particle-like" description of the motion and interaction of crack tips is currently available. However, simplified approaches based on geometry have been used successfully to address crack paths in thin films [7,8]. These models are based on Griffith's theory of fracture [9] *i.e.* total energy (elastic and fracture) minimisation. In the simplest limit of the "inextensible fabric model" [7,10], the pattern can usually be determined by a purely geometric approach in a variety of cases, including the peeling of a thin strip from an adhering substrate or the tearing through a thin film by a blunt object. Even complicated crack paths such as oscillating or spiralling cracks can be understood from this simple model. This approach, however, does not address the variation of the pattern with the elastic properties of the material. Such dependence can be captured by a strict application of total energy minimisation [8]. In this framework, an evaluation of the elastic energy stored in a sample, generally neglecting the detail of the stress field near the crack tip, is needed.

We will be discussing the physics of patterns, a topic familiar to Pierre Coullet, to whom we dedicate this paper, and more precisely the selection of a pattern by a pair of expanding cracks, highlighting the role of the material properties of the sample. The pattern of interest involves two cracks that are formed simultaneously when a blunt object tears a thin film of a material. This configuration is often called the *concertina* tearing, because the material that is left between the two cracks buckles and folds as does a concertina [11,12]. We rely on a simple experiment that can be conducted by hand and

* Corresponding author.
E-mail address: nicolas.vandenberghe@univ-amu.fr (N. Vandenberghe).

https://doi.org/10.1016/j.crme.2019.03.013

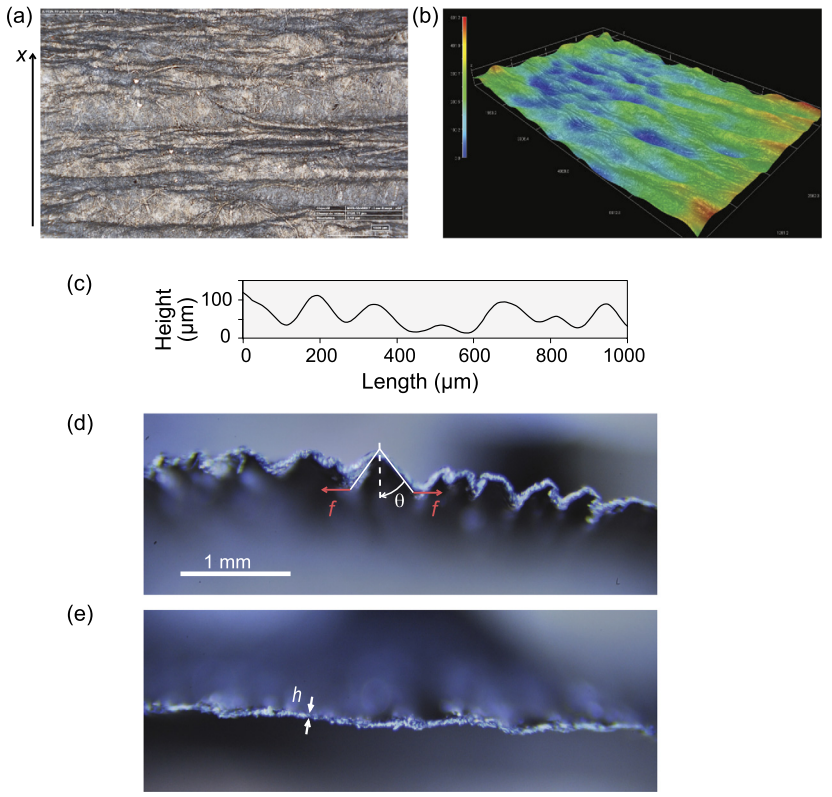

Fig. 1. 3D structure of crepe paper revealing the structure made of ridges and troughs. (a) A view of the surface, (b–c) measurement of the height profile. Note that the z direction is not to scale. (d–e) A cut through an unstretched (d), and stretched (e) sheet of crêpe paper, along with the definitions of the variables entering our analysis.

use a commonly available material (crêpe paper). The material properties and in particular its stiffness can be tuned at will by initially straining the samples, while their fracture energy is constant, independent of the initial strain. We show that the pattern changes dramatically as the stiffness is varied over a broad range. We propose a geometrical model to estimate the total energy of the cracking material, which compares favourably with the observations.

2. Material properties

2.1. Material characterization

We conduct experiments on thin sheets of crêpe paper (Canson brand, typical density 32 g·m^{-2}, thickness in the range from 60 to 100 μm). Crêpe paper is a material used for the creation of artwork. It consists of thin paper that is folded in one direction, thus creating troughs and bumps. The paper is coated with a glue-like substance that holds the pattern of folds. A visualisation of its 3D structure was performed with a 3D-Microscope (Fig. 1) revealing a corrugation of the plate with a typical peak-to-peak amplitude of 80 μm and a wavelength of 180 μm.

A mechanical tensile test has been performed on a testing machine on thin strips of crêpe paper (typical width 10 mm and length 100 mm). Due to the preferred direction of the folds, when pulled upon, the response of the sample presents a strong anisotropy. When stretched in the direction parallel to the direction of trough and ridges, the sample presents a classical linear elastic response with a stretching modulus $Eh = 65$ N/mm. When stretched in the direction normal to the folds, the sample is much softer and it presents a strong nonlinear response as shown in Fig. 2. The response is characterized by different features. First if one considers the stress–strain relation itself (i.e. the upper envelope of the curve in Fig. 2 omitting the presence of unloading cycles), we note that it is similar to the curve obtained in other materials formed by networks of elastic components such as rubber [13] or folded paper [14]. The loading curve presents a marked softening at intermediate strains, while at higher strains the material gets stiffer. An observation of the material after the pulling test (Fig. 1d,e) reveals that the morphology of the stretched sample changes: the amplitude of the corrugation has been reduced, indicating plasticity in the mechanical response of the sample. Then we also note that the unloading–loading cycles performed during the testing of the sample reveal an hysteretic behaviour characteristic of plasticity. Finally, it is worth noting that the maximal strain attained during testing (after which the sample breaks) is compatible with the profile measurement: the unfolded length is typically

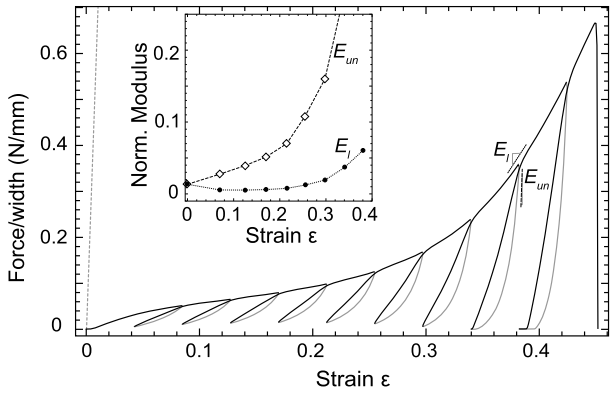

Fig. 2. Measured loading curve for a strip of crêpe paper (width 10 mm, length 100 mm) loaded in the direction perpendicular to its folds (force applied along the x direction). Unloading performed at regular interval during loading reveals a plastic behaviour, even at moderate strain. The gray curves correspond to unloading phases. The steep dashed line shows the elastic behaviour when stretching in the direction parallel to the folds (obtained in a distinct test). The inset shows the local slopes of the loading curve (disks) and of the unloading curves (diamonds) obtained at different strains. The apparent moduli are normalised by the stretching modulus $Eh = 65$ N/mm.

$$l_{\rm un} = \int_0^{l_{\rm ap}} \sqrt{1 + w'(x)^2}\, {\rm d}x \tag{1}$$

where $l_{\rm ap}$ is the apparent length (in the x direction) of the profile $w(x)$. With, for instance, $w(x) = a\sin(2\pi x/\lambda)$, the maximal strain $l_{\rm un}/l_{\rm ap} - 1$ is approximately $(\pi a/\lambda)^2$, yielding approximately 0.5 with $a = 80$ µm and $\lambda = 180$ µm (Fig. 2).

The response of the material in the direction perpendicular to the folds is thus characterised by an apparent stretching modulus that depends on the strain. Two different moduli can be distinguished: a modulus $E_{\rm l}$ obtained by measuring the slope during the loading phase and an unloading modulus $E_{\rm un}$ obtained by measuring the slope during the unloading one. These two quantities are plotted in the inset of Fig. 2.

2.2. Discrete model

The behaviour observed in Fig. 2 can be qualitatively reproduced using a simple model of an elastoplastic ridge (a discrete version of the creased sheet model [15]). We build a model upon an element consisting of two rigid plates of length ℓ merging at a ridge; it will be further convenient to assimilate the ridge to a hinge characterized by a spring constant k and a yield moment m_y above which the rest state of the hinge is modified.

When extended to an angle θ, the moment of the ridge linearized around θ_0 is $m = k(\theta - \theta_0)$ (where k is typically related to the sheet bending stiffness through $k \approx Eh^3/12\ell$) in the elastic domain (*i.e.* $m < m_y$). In the plastic domain, the ridge moment is $m = m_y$ and, if the angle is extended above m_y/k, the rest angle θ_0 increases up to $\theta_0 = \theta - m_y/k$. The force is

$$f = \frac{m}{\ell\cos\theta} \tag{2}$$

and thus as the angle θ increases, the stiffness increases by a purely geometrical effect. In a typical pulling test, starting from the rest state $x = x_0$, for which $f = 0$, as $x = x_0(1+\epsilon)$ is increased, the moment increases, first reaching the yield moment. At this point, the strain–load curve presents a slope change. As the strain ϵ further increases, the moment is constant, $m = m_y$, but the rest angle of the spring increases. The pulling force during the plastic phase of the test is then $f = (m_y/\ell)\,[1 - (x/\ell)^2]^{-1/2}$ and the associated stiffness $\partial f/\partial\epsilon$ in the loading phase when the stress has reached ϵ_1 is

$$k_p = \frac{m_y}{\ell^2}\left(\frac{x_0}{\ell}\right)^2 \frac{1+\epsilon_1}{[1-(x_0/\ell)^2(1+\epsilon_1)^2]^{3/2}} \tag{3}$$

The stiffness increases with ϵ_1 (that is, increasing θ) and this stress hardening is purely geometrical, as seen from Eq. (2). The stiffness in this phase does not depend on the elastic constant k. When the strain has reached ϵ_1, the rest angle of the hinge is $\theta_1 = \arcsin[(x_0/\ell)(1+\epsilon_1)] - m_y/k$.

If starting from ϵ_1 the structure is unloaded (*i.e.* x is lowered), the structure reacts elastically because the moment at the hinge decreases below m_y. The force is now $f = (k/\ell)\{\arcsin[(x_0/\ell)(1+\epsilon)] - \theta_1\}[1-(x/\ell)^2]^{-1/2}$ and thus the stiffness is

$$k_u = \frac{k}{\ell}\frac{(m_y/k)(x_0/\ell)^2(1+\epsilon_1) + (x_0/\ell)[1-(x_0/\ell)^2(1+\epsilon_1)^2]^{1/2}}{[1-(x_0/\ell)^2(1+\epsilon_1)^2]^{3/2}} \tag{4}$$

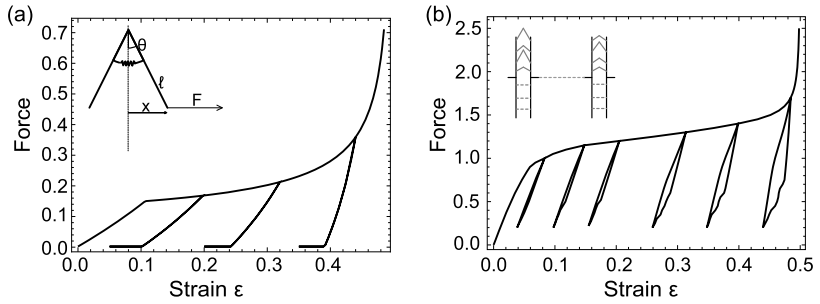

Fig. 3. (a) Mechanical response of a single elastoplastic hinge with x_0/ℓ = 0.67 and $m_y = 0.1$. The response exhibits the softening characteristic of the plasticity and the geometrical stiffening at high strains, when the hinge flattens. (b) When pulled upon, an assembly of hinges displays a behaviour qualitatively similar to that of crepe paper. The curve is obtained for a sequence of 20 elements formed of 30 hinges whose lengths are normally distributed (with a mean 1 and a standard deviation 0.25).

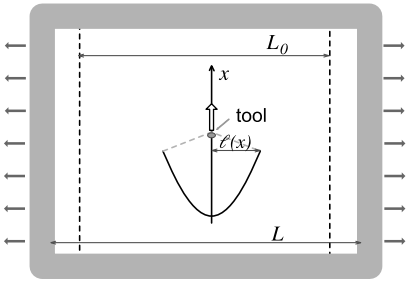

Fig. 4. A tool is used to tear a sheet of crepe paper, starting from a small notch. As the tool is pulled, two crack opens, and the pattern can be parameterised by its half-width $\ell(x)$. The sheet of crepe paper can be initially stretched in the direction normal to x (the fold of the paper are in the x direction) by adjusting L. The initial stretching is $\epsilon_0 = (L - L_0)/L_0$.

Thus this single elastoplastic ridge partly reproduces some the behaviour of crepe paper; geometry induces a stiffening of the structure; and unloading during the pulling test implies an elastic response that results in unloading cycles with an apparent stiffness that increases with the strain. (See Fig. 3.)

However, this simple model does not reproduce the hysteretic behaviour observed during the unloading loop. When the wedge is unloaded and then loaded again, the force–displacement curve follows the same path.

The model can be further extended by considering an assembly of hinges in parallel and in sequence, with distributed segment length ℓ. Though the model presents a more constrained geometrical organisation than an actual creased sheet, it shares some of its features: the geometry of a single hinge mimics the geometric nonlinearity of the elastic response of a fold, and the plasticity introduced at the hinge is similar to the plasticity observed on the crêpe paper sheet. Even though a quantitative comparison is out of the scope of the present paper, it is worth noting that pulling an assembly of hinges with distributed lengths (all other parameters being uniform) leads to a behaviour qualitatively similar to that of crêpe paper. In particular, it exhibits the stress softening associated with plasticity, the stress hardening at high strains associated with the flattening of the hinges. It also exhibits the stiffening of the unloading curves as the strain increases, which is associated with the hinges deforming plastically into flatter configurations.

3. Tearing behaviour

3.1. The concertina tearing

We are now interested in the signature of the stress–strain behaviour presented above on crack patterns. Of particular interest is the role of the change of the local stretching modulus on the pattern. The experiment is conducted on sheets of crêpe paper (170 mm × 170 mm) attached to a rigid substrate by a rigid tape (Fig. 4). An initial cut of about 2 mm is performed with a sharp blade on the sheet. A tool of small size (a few millimetre wide at the contact with the paper) is then introduced in the notch and is pulled towards $x > 0$. The setup allows for an adjustment of the initial tension in the x direction. The initial stretching $\epsilon_0 = (L - L_0)/L_0$ can be adjusted between 0 up to 0.4. The width of a sample is 150 mm before application of the stretching.

As the tool is pulled, it tears the sheet of crepe paper. Two cracks extend, leaving a diverging pattern of cracks (Fig. 1). In the domain around the crack tips and the tool, the thin paper is strongly folded (thus the name Concertina tearing [11,12]). As seen in Fig. 5, the half-width of the crack pattern can be approximated by the shape

$$\ell(x) \sim a\, x^{3/4} \tag{5}$$

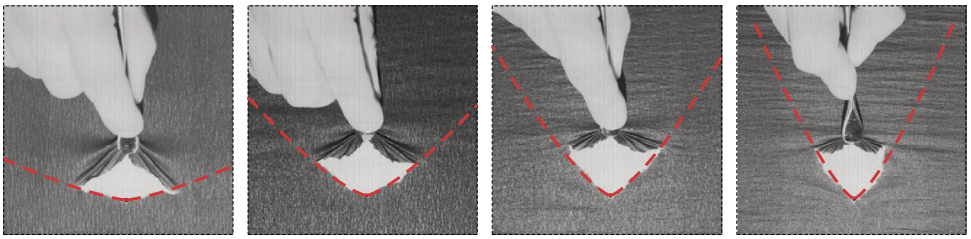

Fig. 5. The crack pattern when a tool is pulled through a sheet of crêpe paper. The four pictures correspond to four different initial stretching levels, from left to right: $\epsilon_0 = 0.053$, 0.21, 0.26, 0.40. The red dashed line indicates a shape $\ell(x) \sim x^{3/4}$. The other experimental conditions are kept identical.

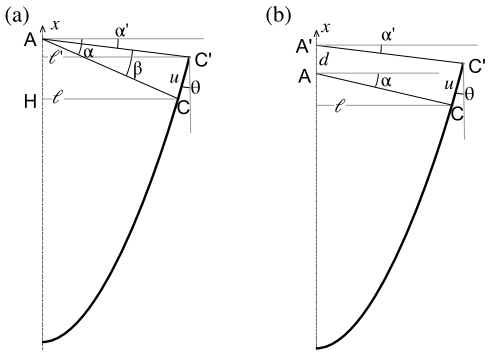

Fig. 6. (a) Sketch of crack extension. The tool is localised in A. The geometry is used to compute the change in strain energy as the crack tip is moved from C to C'. (b) Sketch of crack extension as the tool advances. As the tool advances from A to A', the crack tip moves from C to C'.

This shape is suggested by the theoretical arguments developed in the next section, which also provide the missing dimensional length a^4 in Eq. (5). Remarkably, there is a strong influence of the initial stretching: pre-stretching the material leads to narrower patterns.

4. Geometry of the crack pattern

Modelling is based on Griffith's linear elastic fracture mechanics and follows the analysis of refs. [7,8]. Such an approach requires the calculation of the variation of elastic energy stored in the material during loading and we will assume that this energy is stored in stretching only (*i.e.* the bending energy associated with the folding is neglected). Moreover, in Griffith's approach, the change of elastic energy that occurs during the extension of a crack is associated with unloading. For this reason, we consider that the relevant elastic energy writes $U_s \sim \int E_{\text{un}} h \epsilon^2 \mathrm{d}S$ where $E_{\text{un}}h$ characterises the sample unloading at a given pre-stretch and ϵ is the strain.

The first task is the computation of the strain associated with a given geometry. Consider the crack geometry of Fig. 6a. The tearing force is applied to point A towards $x > 0$ at the apex of the pattern. The segment AC of initial length ℓ is stretched to a length $\ell/\cos\alpha$ and thus the strain is $\epsilon = 1/\cos\alpha - 1$. The analysis proceeds in two stages: first we consider that the angle θ is known and we compute the position of the crack tip (parameterised by the angle α) that ensures that the total energy is minimal. Then an optimisation among all the crack path (*i.e.* the different values of θ) is used to find the actual shape of the pattern.

As the crack tips advances from C to C', the elastic energy is reduced, whereas the crack advance results in an increase of fracture energy. Parameterising the crack advance by the (small) angle $\beta = \alpha - \alpha'$, we can compute the lengths ℓ' and u using the following relations:

$$\ell \tan\alpha - \ell' \tan(\alpha - \beta) = \frac{\ell' - \ell}{\tan\theta}, \quad \text{and} \quad u = \frac{\ell' - \ell}{\sin\theta} \tag{6}$$

yielding (for β small)

$$\ell' = \ell\,[1 + \beta \tan\alpha + \beta \tan(\theta - \alpha)] \quad \text{and} \quad u = \frac{\ell\beta}{\cos\alpha \cos(\theta - \alpha)} \tag{7}$$

The variation of total energy (sum of elastic and fracture energy) is $\delta U \sim E_{\text{un}} h \epsilon'^2 l'^2 - E_{\text{un}} h \epsilon^2 l^2 + \Gamma h u$ with the geometrical parameter β can be computed using Eq. (7). Imposing $\delta U = 0$ at first order as β changes yields an equation for α

$$\cos\alpha - 8\frac{\ell}{c}\cos\left(\frac{\alpha}{2} - \theta\right)\sin^3\frac{\alpha}{2} = 0 \tag{8}$$

where

$$\frac{\ell}{c} = \frac{E_{\mathrm{un}} h\, \ell}{\Gamma h} \tag{9}$$

is a non-dimensional parameter typically found in crack pattern problems: it is the ratio between the characteristic length of the problem ℓ and the material length $c = \Gamma/E_{\mathrm{un}}$ that was put forward in ref. [8].

When $\ell \gg c$, α is small and is approximated by

$$\alpha^3 = \frac{c}{\ell \cos\theta} \tag{10}$$

Equation (8) or its simplified form (10) sets the position of the crack tip whenever the angle θ is known.

We now consider the energy involved as the tool drives the crack. As the tool advances by a distance d (see Fig. 6b), the geometry of the pattern is given by

$$u\cos\theta + \ell' \tan\alpha' = d + \ell\tan\alpha \quad \text{and} \quad u = \frac{\ell' - \ell}{\sin\theta} \tag{11}$$

Combining the two equations, and writing $\ell' = \ell(1+\lambda)$, for α small, one obtains

$$\lambda \approx \frac{d}{\ell}\tan\theta \left[1 + \frac{2}{3}\left(\frac{c}{\ell\cos\theta}\right)^{1/3}\tan\theta\right]^{-1} \tag{12}$$

and

$$u = \frac{\lambda\ell}{\sin\theta} = \frac{d}{\cos\theta}\left[1 + \frac{2}{3}\left(\frac{c}{\ell\cos\theta}\right)^{1/3}\tan\theta\right]^{-1} \tag{13}$$

The total energy variation writes $\delta U \sim E_{\mathrm{un}} h l'^2 \epsilon'^2 - E_{\mathrm{un}} h l^2 \epsilon^2 + \Gamma h u$ with

$$\epsilon' = \frac{1}{\cos\alpha'} - 1 \approx \frac{\alpha'^2}{2} \approx \frac{1}{2}\left(\frac{c}{\ell'\cos\theta}\right)^{2/3} \tag{14}$$

With the different geometric quantities, the variation of energy writes

$$\begin{aligned}\frac{\delta U}{E_{\mathrm{un}} h} &\approx \frac{\ell'^{2/3}}{4}\left(\frac{c}{\cos\theta}\right)^{4/3} - \frac{\ell^{2/3}}{4}\left(\frac{c}{\cos\theta}\right)^{4/3} + \frac{\lambda\,\ell\, c}{\sin\theta} \\ &\approx \ell^{2/3}\frac{1}{6}\left(\frac{c}{\cos\theta}\right)^{4/3}\lambda + \frac{\ell c}{\sin\theta}\lambda\end{aligned}$$

To compute the optimal configuration, we consider the value of θ that ensures that $\partial(\delta U)/\partial d$ is minimal when $\delta \to 0$. The coefficient that should be minimized is

$$C_{\mathrm{d}} = \left[\frac{1}{6}\left(\frac{c}{\ell\cos\theta}\right)^{4/3} + \frac{c}{\ell\sin\theta}\right]\tan\theta\left[1 - \frac{2}{3}\left(\frac{c}{\ell\cos\theta}\right)^{1/3}\tan\theta\right] \tag{15}$$

$$\approx \frac{c}{\ell} - \frac{1}{2}\theta\left(\frac{c}{\ell}\right)^{4/3} + \theta^2\left[\frac{c}{2\ell} - \frac{1}{9}\left(\frac{c}{\ell}\right)^{5/3}\right] \tag{16}$$

Minimizing C_{d} with respect to θ yields at leading order

$$\theta = \frac{1}{2}\left(\frac{c}{\ell}\right)^{1/3} \tag{17}$$

This equation can then be used to compute the shape of the crack as it extends: with $\mathrm{d}\ell/\mathrm{d}x = \tan\theta \approx \theta \approx 1/2(c/\ell)^{1/3}$, we obtain for the shape [8]

$$\ell(x) \approx c^{1/4} x^{3/4} \tag{18}$$

where $c = \Gamma h/E_{\mathrm{un}} h = \Gamma/E_{\mathrm{un}}$ is an intrinsic feature of the material.

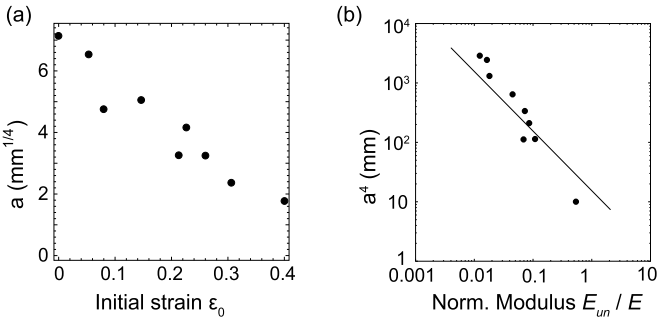

Fig. 7. (a) The variation of the prefactor a of the law $\ell = a x^{3/4}$ for different initial strains ϵ_0 deduced from photographs of the pattern (Fig. 5). (b) The model predicts $a^4 \sim c = \Gamma/E_{\rm un}$, and indeed the plot of a^4 as a function of the unloading modulus is consistent with the model (straight line).

5. Discussion

The shape $\ell = a x^{3/4}$ is consistent with our measurements of the crack pattern observed in experiments (Fig. 5). Moreover, the variation of a with the initial stretching indicates that the variation of the pattern with the initial stretching ϵ_0 is qualitatively consistent with the model: when the sample is stretched, it becomes stiffer and thus the material length c becomes shorter. Therefore, according to Eq. (18), higher values of ϵ_0 should lead to a narrower pattern, as observed in the experiment.

To provide a more quantitative comparison between the model and the experiment, noticing that the fracture energy Γ is not modified by the initial stretching, we use the unloading modulus deduced from the stretching curve (Fig. 2). The variation of the pattern with the initial strain is shown in Fig. 7a. Using the curve for $E_{\rm un}$ to estimate the unloading modulus for each initial strain, it is possible to plot the pre-factor a as a function of the modulus. The results are compared with the expected trend $a^4 \sim c = \Gamma/E_{\rm un}$ in Fig. 7b, and show a fair agreement. The length c, here of the order of 60 mm for $E_{\rm un}/E = 0.1$, corresponds to a fracture energy $\Gamma \approx 10^3$ J/m^2, a standard order of magnitude for paper. We note however that, even though our simple model captures the trend of variation of the pattern with the initial stretching, some ingredients were not included. The exact stress field in the stretched area around the crack tip was not fully computed and, moreover, the unloading modulus only provides a characteristic value for the actual modulus. Such approximations may be responsible for a discrepancy in the evaluation of the elastic energy and thus for the observed discrepancy in Fig. 7b.

To summarize, we have shown that crêpe paper is a particularly interesting material in the sense that it is not only as brittle as paper is, but that its elastic modulus can be tuned over decades thanks to a suitable initial pre-stretch. We have also shown that the concertina tearing test is an easy protocol to access the fracture energy Γ of a material, because its macroscopic pattern is sensitive to a readily measurable length $c = \Gamma/E_{\rm un}$, a length that can, in the case of crêpe paper, be varied over a very broad range.

Acknowledgements

The project leading to this publication has received funding from Excellence Initiative of Aix-Marseille University – A*MIDEX, a French “Investissements d’Avenir” programme. It has been carried out in the framework of the Labex MEC.

References

[1] S. Bohn, J. Platkiewicz, B. Andreotti, M. Adda-Bedia, Y. Couder, Hierarchical crack pattern as formed by successive domain divisions. II. From disordered to deterministic behavior, Phys. Rev. E, Stat. Nonlinear Soft Matter Phys. 71 (4) (2005).
[2] M.L. Fender, F. Lechenault, K.E. Daniels, Universal shapes formed by two interacting cracks, Phys. Rev. Lett. 105 (2010) 125505.
[3] M.-J. Dalbe, J. Koivisto, L. Vanel, A. Miksic, O. Ramos, M. Alava, S. Santucci, Repulsion and attraction between a pair of cracks in a plastic sheet, Phys. Rev. Lett. 114 (2015) 205501.
[4] E. Villermaux, Self-activated fragmentation, Int. J. Fract. 206 (2017) 171–193.
[5] B. Cotterell, J.R. Rice, Slightly curved or kinked cracks, Int. J. Fract. 16 (2) (1980) 155–169.
[6] V. Hakim, A. Karma, Laws of crack motion and phase-field models of fracture, J. Mech. Phys. Solids 57 (2009) 342–368.
[7] B. Roman, Fracture path in brittle thin sheets: a unifying review on tearing, Int. J. Fract. 182 (2) (2013) 209–237.
[8] N. Vandenberghe, E. Villermaux, Geometry and fragmentation of soft brittle impacted bodies, Soft Matter 9 (34) (2013) 8162.
[9] A. Griffith, The phenomena of rupture and flow in solids, Philos. Trans. R. Soc. Lond., Ser. A, Contain. Pap. Math. Phys. Character 221 (1921) 163–198.
[10] T. Tallinen, L. Mahadevan, Forced tearing of ductile and brittle thin sheets, Phys. Rev. Lett. 107 (24) (2011) 245502.
[11] T. Wierzbicki, Concertina tearing of metal plates, Int. J. Solids Struct. 32 (19) (1995) 2923.
[12] T. Wierzbicki, K. Trauth, A. Atkins, On diverging concertina tearing, J. Appl. Mech. 65 (1998) 990.
[13] H. Bouasse, Z. Carrière, Sur les courbes de traction du caoutchouc vulcanisé, Ann. Fac. Sci. Toulouse, 2 Ser. 5 (1903) 257–283.
[14] A. Reid, F. Lechenault, S. Rica, M. Adda-Bedia, Geometry and design of origami bellows with tunable response, Phys. Rev. E 95 (2017) 013002.
[15] F. Lechenault, B. Thiria, M. Adda-Bedia, Mechanical response of a creased sheet, Phys. Rev. Lett. 112 (2014) 244301.